CORA Cork Open Research Archive
Cartlann Taighde Oscailte Chorcaí

Title	Origin of the visible-light response of nickel(II) oxide cluster surface modified titanium(IV) dioxide
Authors	Iwaszuk, Anna;Nolan, Michael;Jin, Qiliang;Fujishima, Musashi;Tada, Hiroaki
Publication date	2013-01-24
Original Citation	Iwaszuk, A., Nolan, M., Jin, Q., Fujishima, M. and Tada, H. (2013) 'Origin of the Visible-Light Response of Nickel(II) Oxide Cluster Surface Modified Titanium(IV) Dioxide', The Journal of Physical Chemistry C, 117(6), pp. 2709-2718. doi: 10.1021/jp306793r
Type of publication	Article (peer-reviewed)
Link to publisher's version	http://pubs.acs.org/doi/abs/10.1021/jp306793r - 10.1021/jp306793r
Rights	© 2013 American Chemical Society. This document is the Accepted Manuscript version of a Published Work that appeared in final form in The Journal of Physical Chemistry C, copyright © American Chemical Society after peer review and technical editing by the publisher. To access the final edited and published work see http://pubs.acs.org/doi/abs/10.1021/jp306793r
Download date	2026-10-30 16:56:19
Item downloaded from	https://hdl.handle.net/10468/1595

UCC
University College Cork, Ireland
Coláiste na hOllscoile Corcaigh

THE JOURNAL OF PHYSICAL CHEMISTRY C

Article

pubs.acs.org/JPCC

Origin of the Visible-Light Response of Nickel(II) Oxide Cluster Surface Modified Titanium(IV) Dioxide

Anna Iwaszuk,[†] Michael Nolan,*[,†] Qiliang Jin,[‡] Musashi Fujishima,[‡] and Hiroaki Tada*[,‡]

[†]Tyndall National Institute, University College Cork, Lee Maltings, Prospect Row, Cork, Ireland

[‡]Department of Applied Chemistry, School of Science and Engineering, Kinki University, 3-4-1, Kowakae, Higashi-Osaka, Osaka 577-8502, Japan

Supporting Information

ABSTRACT: A number of NiO clusters have been formed on TiO_2 (anatase/rutile = 4/1 w/w, P-25, Degussa) in a highly dispersed state (NiO/TiO_2) by the chemisorption−calcination cycle technique. The NiO/TiO_2 causes high visible-light activities for the degradations of 2-naphthol and *p*-cresol exceeding those of FeO_x/TiO_2 (Tada et al. *Angew. Chem., Int. Ed.* **2011**, *50*, 3501−3505). The main purpose of this study is to clarify the origin at an electronic level by the density functional simulation for NiO, Ni_2O_2, and Ni_4O_4 clusters supported on TiO_2 rutile (110) and anatase (001) surfaces. The clusters adsorb strongly on both rutile and anatase with adsorption energies ranging from −3.18 to −6.15 eV, creating new interfacial bonds between the clusters and both surfaces. On rutile, intermetallic Ni−Ti bonds facilitate stronger binding compared with anatase. The electronic structure shows that the top of the valence bands (VBs) of rutile and anatase arises from electronic states on the NiO cluster. On the other hand, the conduction band of rutile is from the Ti 3d states, whereas NiO cluster levels are generated near the conduction band minimum of anatase. This is in contrast to the SnO_2/rutile TiO_2 system, where the density of states near the conduction band minimum increases with the VB unmodified. In the NiO/TiO_2 system, the band gaps of both rutile and anatase are narrowed by up to 0.8 eV compared with pristine TiO_2, which pushes the photoactivity into the visible region. In view of the calculated electronic structure, we have attributed the enhanced photocataltyic activity both to the charge separation due to the excitation from the Ni 3d surface sub-band to the TiO_2 conduction band and the action of the NiO species as a mediator for the electron transfer from the TiO_2 conduction band to O_2.

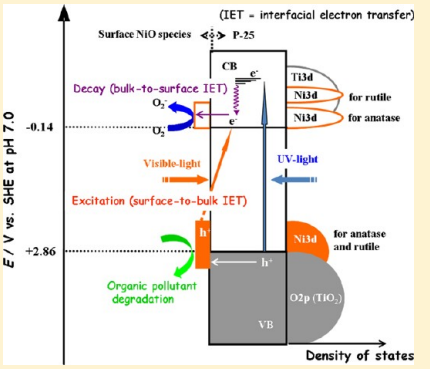

1. INTRODUCTION

One of the biggest challenges for our energy security is to be independent of fossil fuels, and the development of suitable photocatalysts may help in solar energy harvesting. TiO_2 has gathered much attention because it is relatively cheap, readily available, stable, and nontoxic. Since TiO_2 absorbs only in the ultraviolet region, there have been many attempts to modify it in such a way that it will also absorb visible light.[1,2] A popular approach for material modification over many years has been substitutional cation or anion doping at titanium or oxygen sites.[3−19] In 2001, Asahi et al. demonstrated that N-doping of TiO_2 results in visible light absorption,[3] and there has been much work since devoted to examining doping as a means to shifting the band gap of TiO_2 from the UV to the visible. N-doped TiO_2 continues to be of great interest and has been studied in depth by Di Valentin, Pacchioni, and Selloni in refs 4 and 5, while there have been recent experimental and modeling reports on this prototype of doped TiO_2.[6,7] Carbon-doped TiO_2 has also been of great interest,[8−11] while Wang and Lewis have used the FIREBALL code to study doping of TiO_2[12,13] and obtained results that were used to explain the band gap changes in doped TiO_2. Finally, other studies of doped TiO_2 in refs 14−19 serve to highlight the range of dopants that have been studied.

It has been highlighted that there are practical questions associated with doping of TiO_2, including solubility, stability, determining that doping has actually taken place, and charge recombination.[20,21] Herrmann has shown that Cr-doping of TiO_2, which does reduce the band gap, will in fact have a detrimental effect on the photocatalytic activity.[22] With this in mind, there have been many efforts to find alternative ways to shift the band gap of TiO_2 in order to make it more efficient in terms of visible-light absorption and reducing charge recombination. This includes modification with metal particles, such as gold,[21] modification with quantum dots, for example, CdS[23] (which, although displaying an initially high photocatalytic efficiency, does subsequently degrade as a result of CdS oxidation), and heterostructures of graphene and TiO_2[24]

Recent studies have demonstrated that oxide−oxide heterostructures composed of nanoscale metal oxide clusters on TiO_2 can drastically improve the photocatalytic properties

Received: July 9, 2012
Revised: January 23, 2013

 © XXXX American Chemical Society dx.doi.org/10.1021/jp306793r | *J. Phys. Chem. C* XXXX, XXX, XXX−XXX

compared to pure TiO_2.[25−31] Modification of TiO_2 with metal oxide nanoclusters has been investigated by Libera et al.[29] and Tada et al.[30,31] Libera et al. used the atomic layer deposition technique to deposit Fe_2O_3 nanoclusters on TiO_2 and found visible-light absorption and efficient photocatalytic degradation of methylene blue.[29] Tada et al. synthesized FeO_x-modified TiO_2 using the chemisorption−calcination cycle (CCC) that deposits highly dispersed metal oxide nanoclusters on the TiO_2 surface at a molecular scale.[30] The FeO_x/TiO_2 structure shows improved visible-light activity and also good UV-light activity. These features came from band gap narrowing and were explained by the presence of the FeO_x clusters that are responsible for shifting the valence band (VB) maximum of TiO_2.[31] Further, with SnO_2-modified TiO_2, striking differences between the light absorption properties and the visible-light photocatalytic activity of modified rutile and anatase TiO_2 were observed and rationalized with first-principles simulations.[32,33]Other examples of heterostructures have included $BiOBr−ZnFe_2O_4$,[27] $BiVO_4−WO_3$,[28] $SnO_x−ZnGa_2O_4$,[34] and $AgI−BiO$,[35] displaying improved photocatalytic activity compared to the pure oxides or simple physical mixtures, highlighting the important role of the interface.[35] Further, the Ni^{2+} surface modification of rutile TiO_2 by the impregnation method was reported to enhance both the UV- and visible-light activities, whereas the effect is much smaller than that by the Fe^{3+} surface modification.[36] Recently, we have shown that the surface modification of TiO_2 with extremely small NiO clusters by the CCC technique (NiO/TiO_2) causes a high visible-light activity concomitantly with the UV-light activity increased for the decomposition of 2-naphthol.[37] However, the origin of the visible-light response is not fully understood and needs further investigation to facilitate the development of this exciting approach to developing photocatalytic materials.

On the other hand, to understand the origin of the experimental findings, density functional theory (DFT) simulations are of great help. Iwaszuk and Nolan have shown that that subnanometer diameter $(TiO_2)_n$ clusters, with $n = 2−4$, adsorbed on the rutile $TiO_2(110)$ surface, can reduce the band gap compared to pure TiO_2 (although that work was also focused on examining the reactivity of these heterostructures).[38] The presence of Ti 3d states of the cluster above the VB will enhance charge separation, and the photocatalytic activities will be improved.[38] Moreover, further work has demonstrated that modification of TiO_2 with other transition metal oxides will also result in potentially useful photocatalytic properties. For example, DFT simulations show that small transition metal oxide nanoclusters, for example, Cr_2O_3 and Mo_2O_4, deposited on TiO_2 rutile (110) will lead to a band gap reduction[39] and improvement of photocatalytic activities. Thus, the surface modification of the catalyst is an approach that may benefit over doping by reducing formation of localized electronic states and electron/hole recombination that are the key factors for an efficient photocatalyst.

Herein, we report that NiO/TiO_2 (anatase/rutile = 4/1 w/w, specific surface area = 50 $m^2\ g^{-1}$, P-25, Degussa) exhibits high levels of visible-light activities for 2-naphthol and *p*-cresol degradations concurrently with enhanced UV-light activity. P-25 possesses high UV-light activity for the degradation of most organic compounds. Furthermore, in elucidating the origin of the activity of NiO-modified TiO_2, we show by spectroscopic measurements and DFT calculations that the visible-light response of modified TiO_2 is induced by the rise in the VB top with NiO surface modification. We investigate the TiO_2 anatase (001) and rutile (110) surfaces modified with NiO nanoclusters using DFT simulations to establish (1) how NiO nanocluster modification of TiO_2 changes the light absorption properties and (2) if there is any sensitivity to TiO_2 crystal form, as observed for SnO_2.[33] We investigated representative structures of NiO, Ni_2O_2, and Ni_4O_4 nanoclusters deposited on both TiO_2 surfaces. All NiO clusters adsorb strongly on both surfaces; however, adsorption is stronger at the rutile (110) surface due to formation of additional Ni−Ti metallic bonds that are not possible at the anatase (001) surface. The electronic structure shows that the band gap is narrowed and the energy band alignments will give electron and hole separation after light excitation.

2. METHODOLOGY

2.1. Photocatalyst Synthesis. The NiO/P-25 was prepared by the CCC technique.[30] After P-25 (1 g) had been added to 100 mL of a $Ni(acac)_2(H_2O)_2$ solution (solvent, ethanol/*n*-hexane = 3:17 v/v), they were allowed to stand for 24 h at 298 K. The $Ni(acac)_2(H_2O)_2$ concentration was changed ranging from 1×10^{-5} to $\sim 5 \times 10^{-3}$ M. The resulting samples were washed repeatedly with the solvent for the physisorbed complexes to be removed and dried, followed by heating in air at 773 K for 1 h. The complex adsorption and the subsequent heating were repeated to increase the Ni loading amount. The loading amount was shown by the amount of Ni loaded on the unit surface area of P-25 (Γ, ions nm^{-2}).

2.2. Photocatalyst Characterization. High-resolution transmission electron microscopy (HRTEM) observation and X-ray energy dispersive spectroscopic measurements were performed using a JEOL JEM-3000F and a Gatan imaging filter at an applied voltage of 300 or 297 kV. UV−visible diffuse reflectance spectra of NiO/TiO_2 were recorded on a Hitachi U-4000 spectrophotometer. The spectra were converted to the absorption spectra by using the Kubelka−Munk function. X-ray photoelectron spectroscopic (XPS) measurements were performed using a Kratos Axis Nova X-ray photoelectron spectrometer with a monochromated Al Kα X-ray source ($h\nu$ = 1486.6 eV) operated at 15 kV and 10 mA. The takeoff angle was 90°, and multiplex spectra were obtained for Ni 2p, O 1s, and Ti 2p photopeaks. All the binding energies were referenced with respect to the C 1s at 284.6 eV. The photoluminescence spectra were measured with an excitation wavelength of 320 nm at 77 K using a JASCO FP-6000 spectrofluorometer.

2.3. Photocatalytic Reactions. A 50 mL amount of 1.0×10^{-5} M 2-naphthol solution (solvent, acetonitrile/water = 1:99 v/v) or 5.0×10^{-4} M *p*-cresol solution (solvent, water) was placed in a double-jacket-type reaction cell made of borosilicate glass, and then, P-25 (Degussa) or NiO/P-25 particles (0.1 g) were added. The reaction cell was irradiated with a Xe lamp (Wacom XRD-501SW) through a band-pass filter (33U, SIGMA KOKI CO., Ltd.) superposed on FTO-coated glass (two pieces of FTO glass for 2-naphthol and a piece of FTO glass for *p*-cresol) transmitting only the 330−400 nm range for the UV-light photocatalytic activity evaluation and a high-pass filter (L-42, Toshiba) to cut off UV light for the visible-light-induced activity test. The irradiation conditions are as follows: for 2-naphthol UV light, $330 < \lambda < 400$ nm, $I_{320-400\ nm} = 0.5$ mW cm^{-2}, and visible light, $\lambda > 400$ nm, $I_{420-485\ nm} = 1.0$ mW cm^{-2}; for *p*-cresol UV light, $330 < \lambda < 400$ nm, $I_{320-400\ nm} = 2$ mW cm^{-2}, and visible light, $\lambda > 400$ nm, $I_{420-485\ nm} = 2$ mW cm^{-2}. A 3 mL amount of the solution was sampled every 15 min, and the absorbance at $\lambda = 224$ nm was measured using a

dx.doi.org/10.1021/jp306793r | J. Phys. Chem. C XXXX, XXX, XXX−XXX

spectrometer (UV-1800, Shimadzu) to determine the concentration of 2-naphthol. The *p*-cresol concentration was determined by high-performance liquid chromatography (SPD-6A, Shimadzu; column = Fluofix INW425 4.6 mm × 250 mm (NEOS); mobile phase = water−ethanol (3:7 v/v); λ = 277 nm).

2.4. DFT Simulation. For modeling TiO_2 rutile (110) and anatase (001) surfaces, we use three-dimensional periodic slab models with the VASP code.[40] The valence electrons are described by a plane wave basis set, and the cutoff for kinetic energy is 396 eV. The valence electrons are 4 for Ti, 6 for O, and 10 for Ni, within the PAW approximation, and the exchange-correlation functional is the approximation of Perdew−Wang (PW91).[41,42] The Monkhorst−Pack scheme is used for k-point sampling with a (2 × 2 × 1) sampling grid. The rutile (110) surface is terminated by 2-fold coordinated bridging oxygen atoms, and the next sublayer consists of 6-fold and 5-fold coordinated Ti atoms. The (unreconstructed) (001) surface model of anatase is terminated by 2-fold coordinated oxygen and has 5-fold coordinated Ti ions in the next sublayer. We use models of rutile (110) and anatase (001), since (110) is by far the most stable surface of rutile and is well studied,[43] while for anatase, (001) is of great interest as the most photocatalytically active anatase surface.[44,45] We consider the rutile and anatase surfaces in their perfect, stoichiometric form, with consideration of the OH-terminated surfaces that are well known for TiO_2 being the subject of ongoing studies. In order to have isolated NiO nanoclusters, we employed a (2 × 4) surface supercell for each TiO_2 surface; for the largest NiO nanocluster considered, a (4 × 4) rutile (110) surface was also studied to examine the effect of the interaction of NiO clusters with periodic images on the resulting properties, with the larger surface supercell giving a bigger distance between periodic NiO images, thus reducing the periodic interactions and modeling more widely separated NiO nanoclusters. NiO nanoclusters with composition NiO, Ni_2O_2, Ni_3O_3, and Ni_4O_4 are studied as representative molecular-sized NiO nanoclusters. The supercells and technical parameters for the free nanoclusters are the same as the extended surfaces.

For the calculations we use the DFT+*U* approach[46,47] where we applied *U* = 4.5 eV on the Ti 3d states. The need to introduce the *U* parameter in order to describe properly electronic states of d or f shells is well known.[46−50] We also applied the +*U* correction for Ni in NiO, since the electronic states of NiO are known to be poorly described with DFT;[46,47,51−53]for Ni, we apply *U* = 8 eV and *J* = 1 eV (giving *U* − *J* = 7 eV), generally consistent with values from the literature, for example, refs 51−53; a check with other values of *U*, namely, (*U* − *J*) = 5 and 6 eV, gives similar results to those found here for the electronic structure. The DFT+*U* approach gives a reasonable description of transition metal d states, but still an underestimation of band gap remains, and this depends on the precise DFT+*U* setup. With this in mind, the change in the band gap of TiO_2 upon modification with NiO, which is more reliable, is our primary focus.

The clusters were deposited on both TiO_2 surfaces and fully relaxed. The adsorption energy was computed from the following:

$$E^{ads} = E((NiO)_n - TiO_2) - \{E((NiO)_n) + E(TiO_2)\} \quad (1)$$

where $E((NiO)_n - TiO_2)$ is the total energy of the NiO nanocluster supported on the surface and $E((NiO)_n)$ and $E(TiO_2)$ are the total energies of the free cluster and the bare surface, respectively. A negative adsorption energy signifies that the cluster adsorption is stable.

3. RESULTS

The point of effective surface modification of TiO_2 with metal oxide clusters is the dispersion state and the strict control of the loading amount.[30] The $Ni(acac)_2(H_2O)_2$ complex is chemisorbed on P-25 via the partial ligand exchange between the acac ligand and the acidic surface Ti−OH group to yield NiO clusters by postheating.[37] Figure 1 shows HRTEM micrographs

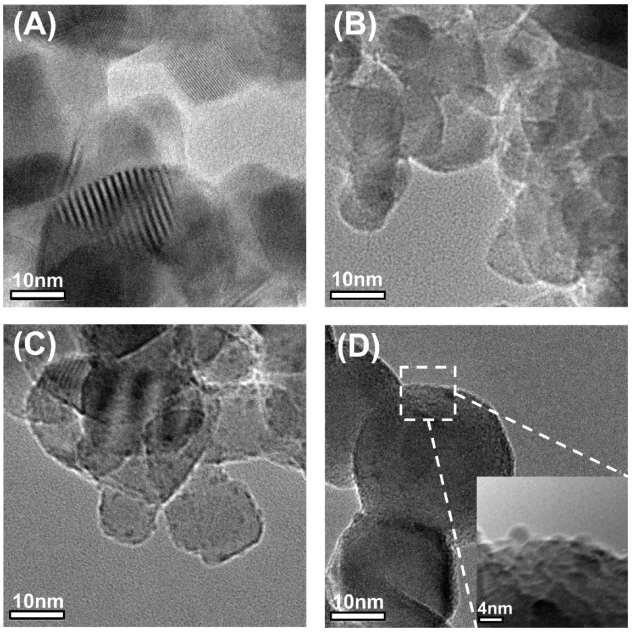

Figure 1. HRTEM images of NiO/P-25: (A) Γ = 0; (B) Γ = 0.014; (C) Γ = 0.47; (D) Γ = 0.83.

of NiO/TiO_2 with varying Ni loading amount Γ (ions nm^{-2}). Highly dispersed NiO clusters smaller than ∼2 nm are observed on the surface of P-25. The strong chemisorption of the complex on the TiO_2surface (DFT results) prevents aggregation of the small NiO clusters into larger structures during the subsequent heating, thus yielding extremely small adsorbed NiO clusters.

2-Naphthol and *p*-cresol were used as model water pollutants. 2-Naphthol, a starting material of azo-dyes, has no absorption at λ > 330 nm.[54] Both the degradations of 2-naphthol and *p*-cresol apparently followed the first-order rate law under irradiation of UV light and visible light, and the activity was evaluated by the pseudofirst-order rate constant (*k*, h^{-1}). Figure 2A (red circles) shows visible-light activity for the 2-naphthol degradation as a function of Γ. The surface modification with NiO clusters endows P-25 with visible-light activity, whereas pristine P-25 has only low activity. The visible-light activity drastically increases with increasing Γ, passing through a maximum at Γ ∼ 0.32. The maximum activities of several metal oxide surface modified P-25 are on the order of NiO > FeO_x > SnO_2 > none under the same reaction conditions, and the value of NiO/P25 reaches approximately twice that of the FeO_x/P-25 system (Table S1, Supporting Information).[30] Figure 2B (red circles) shows UV-light activity for the 2-naphthol degradation as a function of Γ. The UV-light activity further increases by the surface modification with the

dx.doi.org/10.1021/jp306793r | J. Phys. Chem. C XXXX, XXX, XXX−XXX

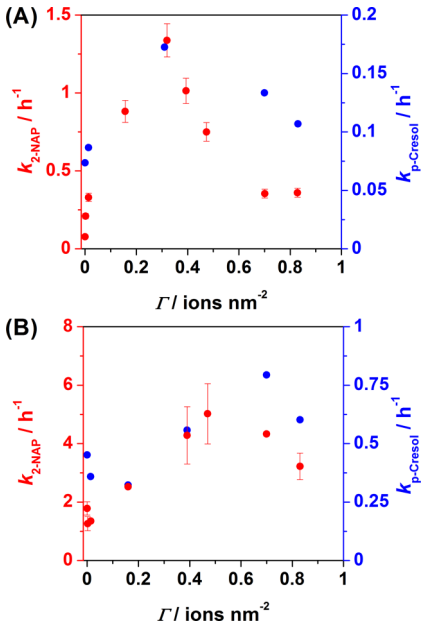

Figure 2. (A) Visible-light and (B) UV-light activities of NiO/P-25 for 2-naphthol (red circles) and *p*-cresol (blue circles) degradations.

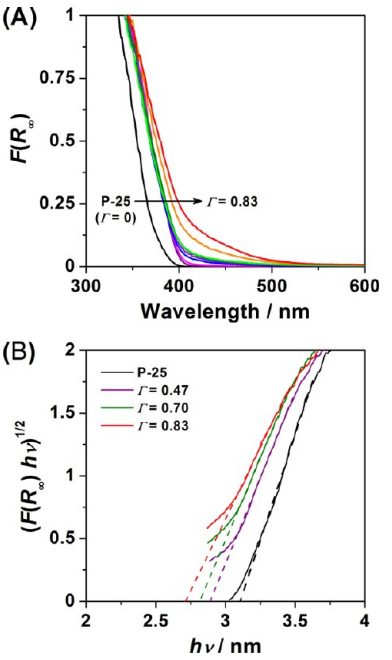

Figure 3. (A) UV−visible absorption spectra of NiO/P-25 with varying Γ: $F(R_\infty)$ denotes the Kubelka−Munk function. (B) Plots of $(F(R_\infty h\nu))^{1/2}$ vs $h\nu$.

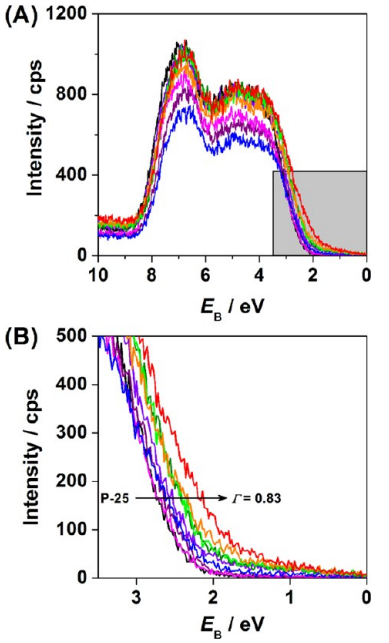

Figure 4. (A) VB-XPS of NiO/P-25 (Γ = 0, 0.0018, 0.014, 0.16, 0.32, 0.39, 0.47, 0.70, and 0.83 from left to right). (B) Magnified VB-XPS near the VB maximum.

NiO clusters. The loading at Γ = 0.47 affords a maximum activity, which is ∼2.8 times the activity of P-25. The maximum activities of several metal oxide surface modified P-25 are on the order of FeO_x > NiO > SnO_2 ∼ none (Table S1, Supporting Information). We have recently reviewed the difference in the surface modification effect between FeO_x and SnO_2 clusters.[55] On the other hand, *p*-cresol widely used as a sterilizer and disinfectant has no absorption at λ > 330 nm. As shown in Figure 2A,B (blue circles), similar trends are also observed for the degradation of *p*-cresol, while the enhancement effect is somewhat smaller as compared to that for the 2-naphthol degradation.

The effect of the surface modification of P-25 with varying amounts of NiO clusters on the optical property was studied. Ni-doped TiO_2 prepared by the solid-state reaction of TiO_2 with NiO has a broad and weak absorption around 450 nm due to the d−d transition, while the intrinsic absorption edge is invariant.[56] Chemical doping of Cr and N ions into TiO_2 yields similar weak shoulders in the visible region due to the formation of localized impurity levels within the band gap.[57]

Figure 3A shows UV−visible absorption spectra of NiO/P-25 with varying Γ: $F(R_\infty)$ is the Kubelka−Munk function. In contrast to the spectra of Ni-doped TiO_2, band gap narrowing occurs for NiO/P-25, whereas the d−d transition band grows at Γ > 0.47. Figure 3B shows plots of $[F(R_\infty)h\nu]^{1/2}$ versus $h\nu$ for NiO/P-25.[58] The indirect band gap determined from the extrapolation of the tangent to the abscissa decreases from 3.1 eV at Γ = 0 to 2.6 eV at Γ = 0.83. A similar spectral feature is observed for Cr-[59] and N-doped[60] TiO_2 prepared by physical techniques such as ion implantation and magnetron sputtering. Also, the VB-XPS was measured for NiO/P-25 with varying Γ. As shown in Figure 4A, the emission from the VB extends from 2 to 9 eV for every sample. Figure 4B magnifies the energy region near the VB maximum. The top of the VB rises with an increase in Γ. The magnitude of the change reaches approximately 0.5 eV at Γ = 0.83, which is comparable with the decrement in the band gap with the surface modification. Consequently, the visible-light absorption of TiO_2 by the surface modification with the NiO clusters stems from the rise in the top of the VB.

To understand the effect of the surface modification with the NiO clusters at an electronic level, DFT simulations were performed for model systems consisting of TiO_2 and NiO nanoclusters adsorbed at rutile and anatase. Figure 5 presents the atomic structure of the NiO, Ni_2O_2, Ni_3O_3, and Ni_4O_4 nanoclusters, which are chosen as representative NiO nanoclusters, adsorbed on TiO_2 anatase (001) and rutile (110) surfaces together with the adsorption energies and the

dx.doi.org/10.1021/jp306793r | J. Phys. Chem. C XXXX, XXX, XXX−XXX

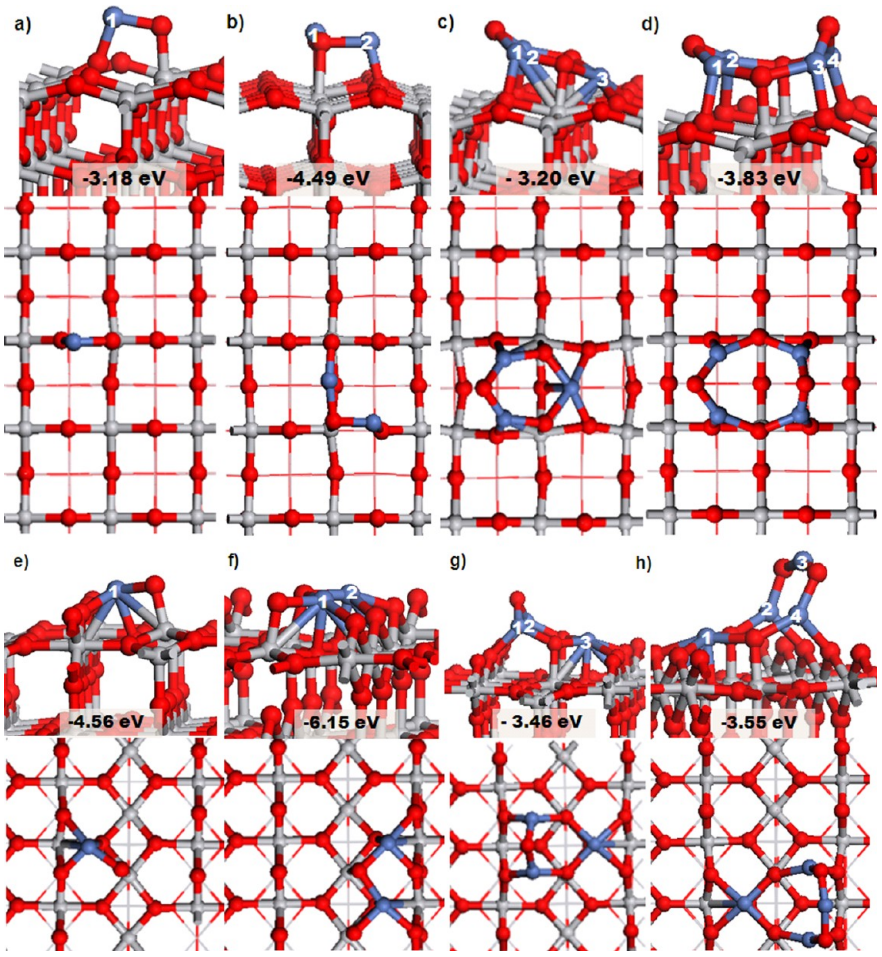

Figure 5. Relaxed adsorption structures with adsorption energies given in eV for (a) NiO, (b) Ni_2O_2, (c) Ni_3O_3, and (d) Ni_4O_4 clusters on TiO_2 anatase (001) and (d) NiO, (e) Ni_2O_2, and (f) Ni_4O_4 clusters on TiO_2 rutile (110). The blue spheres are Ni atoms, the gray spheres are Ti atoms, and the red spheres are O atoms. Cluster Ni atoms are numbered.

numbering of the nanocluster Ni atoms. We compute the coverage of the nanoclusters in terms of Ni atoms per unit area, so that for NiO, Ni_2O_2, Ni_3O_3, and Ni_4O_4 on anatase (001), the coverages are 0.85, 1.70, 2.55, and 3.41 Ni atoms/nm^2. On rutile (110), the corresponding coverages are 0.64, 1.28, 1.92, and 2.56 Ni atoms/nm^2. On the larger (4 × 4) surface supercell, the coverage is 1.28 Ni atoms/nm^2. For Ni_4O_4, the size of the nanocluster on a (2 × 4) surface supercell will lead to stronger periodic NiO−NiO interactions than for the smaller NiO nanoclusters, which will influence the adsorption structure, due to the NiO nanoclusters being essentially in close proximity, and the effect of this on the change in the electronic properties of NiO-modified TiO_2 will be discussed.

All structures show negative adsorption energies, ranging from −3.18 to −6.15 eV giving an indication of a strong interaction between the nanocluster and the surface and the high stability of individual NiO nanoclusters adsorbed at TiO_2, which prevents aggregation of the clusters into larger structures during postheating. For all deposited clusters, detailed information about the geometry is presented in Table 1.

For NiO nanoclusters deposited on anatase, the NiO cluster results in two new bonds with the TiO_2 surface with distances of 1.75 and 1.91 Å. It is important to note that an O atom from the anatase surface is pulled out of the surface by Ni from the cluster by 0.26 Å that distorts the surface of TiO_2 anatase (001), similar to SnO_2 adsorbed at anatase (001).[32] The same behavior is observed for Ni_2O_2 deposited at anatase (001), where in this case the O atom is pulled out of the surface by 0.17 Å upon bonding to Ni. The number of new bonds in Ni_2O_2 deposited on TiO_2 anatase (001) is three. The Ni_3O_3 cluster presents 11 new bonds when deposited on TiO_2 anatase (001). There are five bonds between Ni and O atoms in the range 1.93−2.20 Å while oxygen atoms from the cluster bond to Ti surface atoms with two bonds that are 1.90 Å long. The Ni_4O_4 cluster deposited on TiO_2 anatase (001) shows six new bonds. In this case, the surface O atom is pulled out of the surface by 0.19 Å. Within the Ni−O nanoclusters, the Ni−O distances are notably shorter compared to bulk NiO, for example, 1.95 Å in Ni_4O_4, compared to 2.10 Å in bulk NiO. Of the NiO nanoclusters adsorbed at anatase (001), only the Ni_3O_3 nanocluster shows intermetallic Ni−Ti bonds, with Ni−Ti distances in the range 2.71−2.87 Å, which is consistent with those in the intermetallic NiTi alloy.[61]

At the TiO_2 rutile (110) surface, the NiO cluster bonds to the surface with six new bonds. The Ni atom from the cluster bonds with two bridging O atoms and one surface O atom, and the fourth metal−oxygen bond is from an O cluster atom that bonds to Ti surface atoms. The Ni_2O_2 cluster binds to the surface with nine new bonds. Five metal−oxygen bonds are from Ni cluster atoms to surface oxygen, and the last two are from cluster oxygen to surface Ti. Ni_3O_3 deposition on rutile (110) results in formation of seven new bonds between the

dx.doi.org/10.1021/jp306793r | J. Phys. Chem. C XXXX, XXX, XXX−XXX

Table 1. Surface−Cluster Ni−O Bond Distances for NiO Clusters Adsorbed at the TiO_2 Anatase (001) and Rutile (110) Surfaces[a]

	distance (Å)					
	anatase			rutile		
	Ni_c-O_s	O_c-Ti_s	Ni_c-Ti_s	Ni_c-O_s	O_c-Ti_s	Ni_c-Ti_s
NiO	1.75 (1)	1.91		2.08 (1)	1.80	2.61 (1)
				1.96 (1)		2.81 (1)
				2.03 (1)		
Ni_2O_2	1.73 (2)	1.99		2.10 (1)	1.96	2.79 (1)
		2.22		1.92 (1)	1.78	2.70 (1)
				2.09 (1)		2.58 (2)
				2.02 (2)		
				2.03 (2)		
Ni_3O_3	1.95 (1)	1.90	2.87 (1)	1.97 (1)	1.89	2.73 (3)
	1.93 (2)	1.90	2.85 (2)	1.96 (2)	1.89	2.87 (3)
	2.07 (3)		2.71 (3)	2.20 (3)		2.87 (3)
	2.02 (3)		2.71 (3)	2.20 (3)		
	2.20 (3)			2.05 (3)		
Ni_4O_4	1.95 (1)	1.93		2.21 (1)	1.89	2.74 (1)
	1.92 (2)	1.92		2.22 (1)	1.90	
	1.95 (3)			2.04 (1)		
	1.95 (4)			1.96 (2)		
				1.99 (4)		

[a]The numbers in parentheses are the atom numbers of Ni in each NiO nanocluster.

cluster and surface. Five bonds are between Ni cluster atoms and surface O atoms with the bond distances from 1.96 to 2.20 Å. The other two bonds come from O cluster atoms and Ti surface atoms, and their distance is 1.89 Å. The Ni_4O_4 cluster bonds to the rutile surface with eight new bonds where three of the cluster Ni atoms create four Ni−O bonds with bridging surface O atoms and one surface O atom, with the shortest distance being 1.96 Å and the longest distance being 2.22 Å. The other two bonds are from cluster O binding with surface Ti. In each of these structures, surface Ti atoms are pulled out of the surface after bonding to cluster oxygen. For the example of NiO adsorbed at rutile (110), this Ti is displaced by 0.48 Å.

At the (110) surface, we also observe the formation of new intermetallic Ni−Ti bonds between cluster Ni and surface Ti, with the distances given in Table 1. The Ni−Ti distances we observe are consistent with those in the intermetallic NiTi alloy.[61] Since the adsorption energies of NiO nanoclusters on the rutile (110) surface are more negative compared to those on anatase (001) for a given NiO cluster, we suggest that the presence of the new Ni−Ti bonds plays a role in further stabilization of the heterostructure. The exception is the Ni_3O_3 nanocluster, where Ni−Ti bonds are formed at both TiO_2 surfaces and the adsorption energies are very similar.

f6 Figure 6 shows the electronic density of states projected (PEDOS) on Ni 3d and Ti 3d states for NiO, Ni_3O_3, Ni_2O_2, and Ni_4O_4 clusters adsorbed on anatase (001) (Figure 6a−d) and rutile (110) (Figure 6e−h). PEDOS plots for the O 2p states are shown in the Supporting Information (Figure S1); the Ni 3d states lie near the top of the VB in the clusters and are important in this analysis. The DOS of the clean rutile and anatase TiO_2 surfaces (see the Supporting Information) show the well-known O 2p derived VB, with a Ti 3d contribution, while the conduction band is dominated by the Ti 3d states in both anatase and rutile.

Examination of the PEDOS shows clearly that, upon modification of TiO_2 with NiO nanoclusters, NiO cluster derived states are found laying above the top of the VB edge of the rutile and anatase surfaces, which pushes the VB edge of the composite system to higher energy compared to the bare surfaces. The conduction band of the NiO-modified surfaces can show some dependence on the crystal form of TiO_2. For modified rutile (110), the bottom of the conduction band is dominated by surface Ti 3d states. Interestingly, this is in contrast to the SnO_2/rutile TiO_2 system, where the DOS near the conduction band minimum increases, with the VB unmodified.[32] A close inspection of the conduction band states for anatase indicates that, in some cases, for example, Ni_2O_2, empty NiO cluster levels are generated near the conduction band minimum.

In the NiO/TiO_2 system, the shift of the VB to higher energy has the consequence that the overall band gap of the composite is reduced compared to unmodified TiO_2. We find in the DFT calculations a maximum band gap reduction of 0.8 eV (for Ni_4O_4 at anatase (001)) compared to the unmodified anatase surface, and this shift is qualitatively comparable to the value determined by the VB-XPS, in Figure 4B. This can further be compared with SnO_2/TiO_2, where anatase modification leads to no band gap change, but rutile modification can reduce the band gap.[32] The narrowing of the band gap will induce visible-light absorption in the composite as shown in Figure 3. Thus, upon modification with NiO nanoclusters, NiO states appear above the VB edge of the TiO_2 surface, which pushes the VB up in energy. There is a case in Figure 6, where the Ni_2O_2 nanocluster on anatase appears to also show some empty NiO states just below the anatase conduction band. In general, we can conclude that the NiO modification of TiO_2 will reduce the energy gap by pushing the VB edge up in energy.

f7 We show in Figure 7 the atomic structure and PEDOS of a Ni_4O_4 nanocluster relaxed on the rutile (110) surface with a (4 × 4) surface supercell, which has a coverage of 1.28 Ni atoms/nm^2 and an adsorption energy of −4.50 eV. In this case, although the effect of the smaller coverage of NiO at the surface on the final adsorption structure of the nanocluster at this surface is clear compared to Figure 5f, namely, that the Ni_4O_4 cluster takes a different adsorption structure, the PEODS shows that the impact of modifying TiO_2 with NiO is unchanged, namely, that there are NiO-derived states found at the top of the VB, which will reduce the energy gap compared to unmodified TiO_2.

The oxidation state of the metal oxide surface modifier can also affect the photocatalytic activity of TiO_2.[33] A Bader charge analysis[62] on Ni for the NiO nanoclusters deposited on both surfaces gives net charges on Ni ranging from 8.7 to 8.9 electrons, which are consistent with a Ni^{2+} oxidation state. Moreover, in TiO_2, the computed net Bader charges are approximately +1.3 electrons, which is typical for the Ti^{4+} oxidation state. The oxidation states of Ni and Ti are in agreement with those determined by XPS.[37]

f8 On the basis of these results above, the NiO surface modification effect on the photocatalytic activity of P-25 can be rationalized as follows and indicated in Figure 8. NiO clusters possess a strong interaction with the anatase and rutile surfaces through Ni−O−Ti bonds for anatase and rutile and additional Ni−Ti bonds for rutile. As a result of the mixing of the Ni 3d levels, the VB maximum of TiO_2 rises significantly, while new vacant levels are generated near the conduction band minimum of anatase that is the major phase of P-25.

dx.doi.org/10.1021/jp306793r | J. Phys. Chem. C XXXX, XXX, XXX−XXX

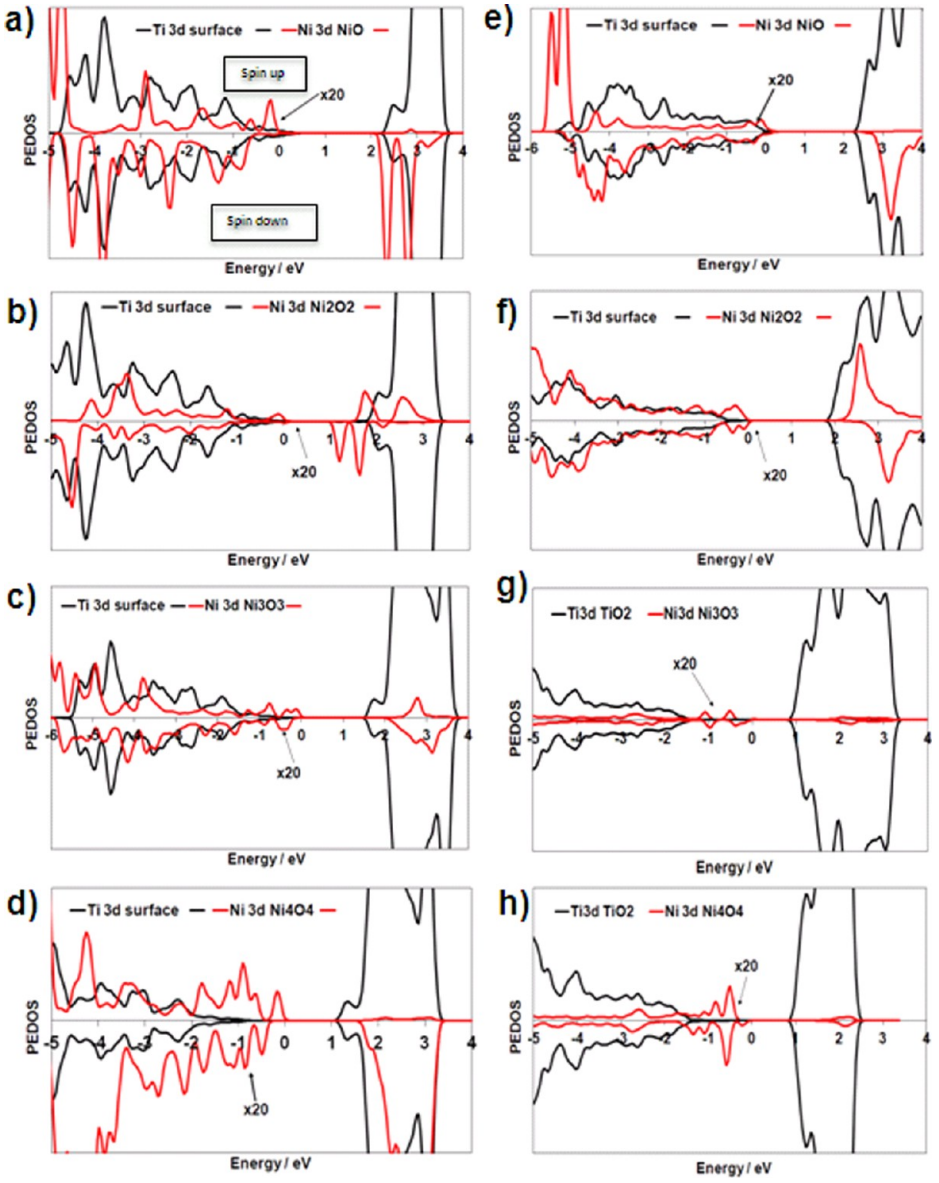

Figure 6. Spin polarized PEDOS on Ni 3d and Ti3d states for (a) NiO, (b) Ni_2O_2, (c) Ni_3O_3, and (d) Ni_4O_4 clusters supported on the anatase (001) surface and for (e) NiO, (f) Ni_2O_2, (g) Ni_3O_3, and (h) Ni_4O_4 clusters supported on the TiO_2 rutile (110) surface.

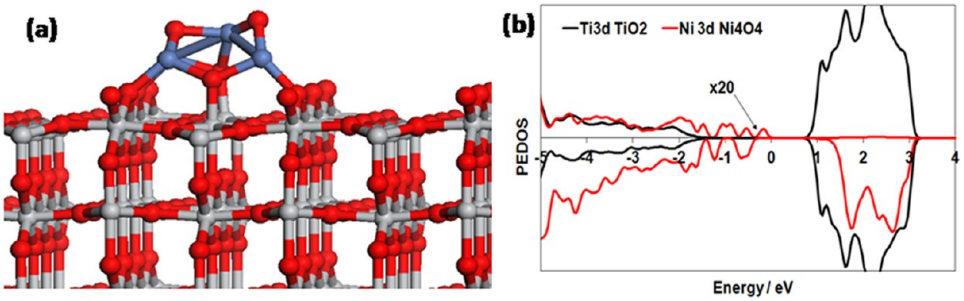

Figure 7. (a) Atomic structure and (b) PEDOS for a Ni_4O_4 cluster adsorbed at the rutile (110) surface in a (4 × 4) surface supercell.

Upon visible-light irradiation of NiO/P-25, the electrons in the surface Ni 3d sub-band are excited to theTiO_2 conduction band. This surface-to-bulk interfacial electron transfer (IET) enhances the charge carrier separation. The holes generated at the surface d sub-band oxidize adsorbed 2-naphthol and *p*-cresol. On the other hand, the electrons in the TiO_2 conduction band are consumed by O_2 reduction. This process can be the key to increasing photocatalytic activity in the oxidative decomposition of organic pollutants.[63,64] Figure 8 suggests that the excited electrons in the anatase conduction band can be transferred to the surface levels of the NiO species, which further assists the electron transfer to O_2 as previously

dx.doi.org/10.1021/jp306793r | J. Phys. Chem. C XXXX, XXX, XXX–XXX

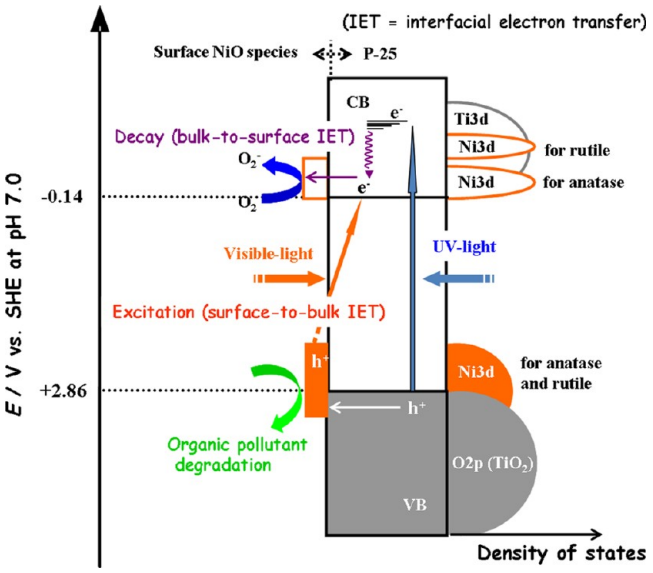

Figure 8. Energy band diagram for NiO-modified TiO_2.

confirmed by the electrochemical experiments.[37] This action mechanism of the NiO clusters should also operate under UV-light irradiation. Consequently, the NiO surface modified P-25 causes the high activities under illumination of visible light and UV light. A final point is that, in the experiments, an optimum Ni loading for photocatalytic activity is found (Figure 2A,B), although above this loading, the NiO−TiO_2 system displays a continuous decrease in the band gap. With the results of this work showing that the increased loading of NiO results in a rise in the VB edge of the composite system compared to unmodified TiO_2, we can explain this finding as follows. The low VB edge in unmodified TiO_2 imparts good oxidative power to the holes formed after light excitation, while an upward shift of the VB edge will weaken the oxidation power of the holes. Thus, with an increase in NiO loading, the VB edge is shifted upward (Figures 3, 4, and 6), which therefore weakens the oxidative power of the holes and results in an optimal loading of NiO on TiO_2. A similar result has been found for other metal oxide nanocluster modified TiO_2,[30−33] indicating that this phenomenon is quite general; that is, there will be an optimum loading of a second metal oxide on TiO_2 that shifts the VB edge such that visible-light absorption is realized but that the oxidative power of the photoexcited holes is not reduced too much.

4. CONCLUSIONS

We have shown that the surface modification of P-25 (anatase/rutile = 4:1 w/w) with NiO clusters gives rise to high visible-light activities for 2-naphthol and *p*-cresol concomitantly with significant increases in the UV-light activities. We have presented DFT simulations of nickel oxide clusters adsorbed on TiO_2 anatase (001) and rutile (110) surfaces to understand the origin of visible-light activity in these heterostructures. We find that NiO clusters are deposited on TiO_2 surfaces with large adsorption energies ranging from −3.18 to −6.15 eV, with metallic Ni−Ti bonds leading to extra stabilization on rutile (110) compared with anatase (001). The deposited clusters cause the narrowing of the TiO_2 band gap, which pushes the photoactivity into the visible region due to the presence of NiO states at the top of the valence band of TiO_2. The present energy level alignments enhance the charge separation and the electron transfer to O_2, which are the origins of photocatalytic efficiency enhancement. These results are consistent with experimental data.

■ ASSOCIATED CONTENT

Supporting Information

Photocatalytic activities of metal oxide surface modified P-25 (Degussa) for 2-naphthol degradation; Ni 3d and O 2p PEDOS for NiO nanocluster modified TiO_2; electronic DOS for unmodified rutile (110) and anatase (001) surfaces. This material is available free of charge via the Internet at http://pubs.acs.org.

■ AUTHOR INFORMATION

Corresponding Author

*E-mail: michael.nolan@tyndall.ie (M.N.); h-tada@apch.kindai.ac.jp (H.T.).

Notes

The authors declare no competing financial interest.

■ ACKNOWLEDGMENTS

M.N. and A.I. acknowledge support from Science Foundation Ireland (SFI) through the Starting Investigator Research Grant Program, project "EMOIN", grant number SFI 09/SIRG/I1620, and computing resources at Tyndall provided by SFI and by the SFI and Higher Education Authority funded Irish Centre for High End Computing. We acknowledge support from the European Union through the COST Action CM1104 "Reducible Oxide Chemistry, Structure and Functions". H.T. acknowledges supports from the Ministry of Education, Science, Sport, and Culture, Japan through a Grant-in-Aid for Scientific Research (C) no. 24550239, and Nippon Sheet Glass Foundation for Materials Science and Engineering, and by Sumitomo Foundation.

■ REFERENCES

(1) Nie, X. L.; Zhou, S. P.; Maeng, G.; Sohlberg, K. Doping of TiO_2 Polymorphs for Altered Optical and Photocatalytic Properties. *Int. J. Photoenergy* **2009**, No. 294042.

(2) Nowotny, J. Titanium Dioxide-Based Semiconductors for Solar-Driven Environmentally Friendly Applications: Impact of Point Defects on Performance. *Energy Environ. Sci.* **2008**, *1*, 556−572.

(3) Asahi, R.; Morikawa, T.; Ohwaki, K.; Aoki, K.; Taga, Y. Visible-Light Photocatalysis in Nitrogen-Doped Titanium Oxides. *Science* **2001**, *293*, 269−271.

(4) Di Valentin, C.; Finazzi, E.; Pacchioni, G.; Selloni, A.; Livarghi, S.; Paganini, M. C.; Giamello, E. N-Doped TiO_2: Theory and Experiment. *Chem. Phys.* **2007**, *339*, 44−56.

(5) Di Valentin, C.; Pacchioni, G.; Selloni, A. Origin of the Different Photoactivity of N-Doped Anatase and Rutile TiO_2. *Phys. Rev. B* **2004**, *70*, 085116/1−085116/4.

(6) Barolo, G.; Livraghi, S.; Chiesa, M.; Paganinin, M. C.; Giamello, E. Mechanism of the Photoactivity under Visible Light of N-Doped Titanium Dioxide. Charge Carriers Migration in Irradiated N-TiO_2 Investigated by Electron Paramagnetic Resonance. *J. Phys. Chem. C* **2012**, *116*, 20887−20894.

(7) Ceotto, M.; Lo Presti, L.; Cappelletti, G.; Meroni, D.; Spadaveccia, F.; Zecca, R.; Leoni, M.; Scardi, P.; Bianchi, C. L.; Ardizzone, S. About the Nitrogen Location in Nanocrystalline N-Doped TiO_2: Combined DFT and EXAFS Approach. *J. Phys. Chem. C* **2012**, *116*, 1764−1771.

(8) Wu, G.; Nishikawa, T.; Ohtani, B.; Chen, A. Synthesis and Characterization of Carbon-Doped TiO_2 Nanostructures with Enhanced Visible Light Response. *Chem. Mater.* **2007**, *19*, 4530−4537.

(9) Park, J. H.; Kim, S.; Bard, A. J. Novel Carbon-Doped TiO_2 Nanotube Arrays with High Aspect Ratios for Efficient Solar Water Splitting. *Nano Lett.* **2006**, *6*, 24−28.
(10) Di Valentin, C.; Pacchioni, G.; Selloni, A. Theory of Carbon Doping of Titanium Dioxide. *Chem. Mater.* **2005**, *17*, 6656−6665.
(11) Graciani, J.; Ortega, Y.; Sanz, J. F. Carbon Doping of the TiO_2 (110) Rutile Surface. A Theoretical Study Based on DFT. *Chem. Mater.* **2009**, *21*, 1431−1438.
(12) Wang, H.; Lewis, J. P. Second-Generation Photocatalytic Materials: Anion-Doped TiO_2. *J. Phys.: Condens. Matter* **2006**, *18*, 421−434.
(13) Wang, H.; Lewis, J. P. Effects of Dopant States on Photoactivity in Carbon-Doped TiO_2. *J. Phys.: Condens. Matter* **2005**, *17*, L209−L214.
(14) Di Valentin, C.; Pacchioni, G.; Onishi, H.; Kudo, A. Cr/Sb Co-Doped TiO_2 from First Principles Calculations. *Chem. Phys. Lett.* **2009**, *469*, 166−171.
(15) Yu, J. G.; Xiang, Q. J.; Zhou, M. H. Preparation, Characterization and Visible-Light-Driven Photocatalytic Activity of Fe-Doped Titania Nanorods and First-Principles Study for Electronic Structures. *Appl. Catal., B* **2009**, *90*, 595−602.
(16) Long, R.; English, N. J. First-Principles Calculation of Synergistic (N, P)-Codoping Effects on the Visible-Light Photocatalytic Activity of Anatase TiO_2. *J. Phys. Chem. C* **2010**, *114*, 11984−11990.
(17) Zheng, J. W.; Bhattcahrayya, A.; Wu, P.; Chen, Z.; Highfield, J.; Dong, Z. L.; Xu, R. The Origin of Visible Light Absorption in Chalcogen Element (S, Se, and Te)-Doped Anatase TiO_2 Photocatalysts. *J. Phys. Chem. C* **2010**, *114*, 7063−7069.
(18) Peng, H. W.; Li, J. B.; Li, S. S.; Xia, J. B. First-Principles Study of the Electronic Structures and Magnetic Properties of 3d Transition Metal-Doped Anatase TiO_2. *J. Phys.: Condens. Matter* **2008**, *20*, 125207.
(19) Bian, L.; Song, M. X.; Zhou, T. L.; Zhao, X. Y.; Dai, Q. Q. Band Gap Calculation and Photo Catalytic Activity of Rare Earths Doped Rutile TiO_2. *J. Rare Earths* **2009**, *27*, 461−468.
(20) Kubacka, A.; Fernandez-Garcia, M.; Colon, G. Advanced Nanoarchitectures for Solar Photocatalytic Applications. *Chem. Rev.* **2012**, *112*, 1555−1614.
(21) Primo, A.; Corma, A.; Garcia, H. Titania Supported Gold Nanoparticles as Photocatalyst. *Phys. Chem. Chem. Phys.* **2011**, *13*, 886−910.
(22) Herrmann, J. M. Detrimental Cationic Doping of Titania in Photocatalysis: Why Chromium Cr^{3+}-Doping is a Catastrophe for Photocatalysis, Both under UV- and Visible Irradiations. *New. J. Chem.* **2012**, *36*, 883−890.
(23) Tada, H.; Mitsui, T.; Kiyonaga, T.; Akita, T.; Tanaka, K. All-Solid-State Z-Scheme in CdS−Au−TiO_2 Three-Component Manojunction System. *Nat. Mater.* **2006**, *5*, 782−786.
(24) Williams, G.; Seger, B.; Kamat, P. V. TiO_2-Graphene Nanocomposites. UV-Assisted Photocatalytic Reduction of Graphene Oxide. *ACS Nano* **2008**, *2*, 1487−1491.
(25) Murakami, N.; Chiyoya, T.; Tsubota, T.; Ohno, T. Switching Redox Site of Photocatalytic Reaction on Titanium(IV) Oxide Particles Modified with Transition-Metal Ion Controlled by Irradiation Wavelength. *Appl. Catal., A* **2008**, *348*, 148−152.
(26) Yu, H.; Irie, H.; Shimodaira, Y.; Hosogi, Y.; Kuroda, Y.; Miyauchi, M.; Hashimoto, K. An Efficient Visible-Light-Sensitive Fe(III)-Grafted TiO_2 Photocatalyst. *J. Phys. Chem. C* **2010**, *114*, 16481−16487.
(27) Hong, S. J.; Lee, S.; Jang, J. S.; Lee, J. S. Heterojunction $BiVO_4$/WO_3 Electrodes for Enhanced Photoactivity of Water Oxidation. *Energy Environ. Sci.* **2011**, *4*, 1781−1787.
(28) Kong, L.; Jiang, Z.; Xiao, T.; Lu, L.; Jones, M. O.; Edwards, P. P. Exceptional Visible-Light-Driven Photocatalytic Activity over BiOBr−$ZnFe_2O_4$ Heterojunctions. *Chem. Commun.* **2011**, *47*, 5512−5514.
(29) Libera, J. A.; Elam, J. W.; Sather, N. F.; Rajh, T. M.; Dimitrijevic, N. M. Iron(III)-Oxo Centers on TiO_2 for Visible-Light Photocatalysis. *Chem. Mater.* **2010**, *22*, 409−413.
(30) Tada, H.; Jin, Q.; Nishijima, H.; Yamamoto, H.; Fujishima, M.; Okuoka, S.-i.; Hattori, T.; Sumida, Y.; Kobayashi, H. Titanium(IV) Dioxide Surface-Modified with Iron Oxide as a Visible Light Photocatalyst. *Angew. Chem., Int. Ed.* **2011**, *50*, 3501−3505.
(31) Jin, Q.; Fujishima, M.; Tada, H. Visible-Light-Active Iron Oxide-Modified Anatase Titanium(IV) Dioxide. *J. Phys. Chem. C* **2011**, *115*, 6478−6483.
(32) Fujishima, M.; Jin, Q.; Yamamoto, H.; Tada, H.; Nolan, M. Tin Oxide-Surface Modified Anatase Titanium(IV) Dioxide with Enhanced UV-Light Photocatalytic Activity. *Phys. Chem. Chem. Phys.* **2012**, *14*, 705−711.
(33) Jin, Q.; Fujishima, M.; Nolan, M.; Iwaszuk, A.; Tada, H. Photocatalytic Activities of Tin(IV) Oxide Surface-Modified Titanium-(IV) Dioxide Show a Strong Sensitivity to the TiO_2 Crystal Form. *J. Phys. Chem. C* **2012**, *116*, 12621−12626.
(34) Boppana, V. B. R.; Lobo, R. F. SnO_x-$ZnGa_2O_4$ Photocatalysts with Enhanced Visible Light Activity. *ACS Catal.* **2011**, *1*, 923−928.
(35) Cheng, H.; Huang, B.; Dai, Y.; Qin, X.; Zhang, X. One-Step Synthesis of the Nanostructured AgI/BiOI Composites with Highly Enhanced Visible-Light Photocatalytic Performances. *Langmuir* **2010**, *26*, 6618−6624.
(36) Murakami, N.; Chiyoya, T.; Tsubota, T.; Ohno, T. Switching Redox Site of Photocatalytic Reaction on Titanium(IV) Oxide Particles Modified with Transition-Metal Ion Controlled by Irradiation Wavelength. *Appl. Catal., A* **2008**, *348*, 148−152.
(37) Jin, Q.; Ikeda, T.; Fujishima, M.; Tada, H. Nickel(II) Oxide Surface-Modified Titanium(IV) Dioxide as a Visible-Light-Active Photocatalyst. *Chem. Commun.* **2011**, *47*, 8814−8816.
(38) Iwaszuk, A.; Nolan, M. Reactivity of Sub 1 nm Supported Clusters: $(TiO_2)_n$ Clusters Supported on Rutile TiO_2 (110). *Phys. Chem. Chem. Phys.* **2,011**, *13*, 4963−4973.
(39) Nolan, M. Surface Modification of TiO_2 with Metal Oxide Nanoclusters: a Route to Composite Photocatalytic Materials. *Chem. Commun.* **2011**, *47*, 8617−8619.
(40) Kresse, G.; Hafner, J. Ab Initio Molecular-Dynamics Simulation of the Liquid-Metal-Amorphous-Semiconductor Transition in Germanium. *Phys. Rev. B* **1994**, *49*, 14251−14269.
(41) Blöchl, P. E. Projector Augmented-Wave Method. *Phys. Rev. B* **1994**, *50*, 17953−17979.
(42) Perdew, J. P. In *Electronic Structure of Solids '91*; Ziesche, P., Eschrig, H., Eds.; Akademie Verlag: Berlin, Germany, 1991.
(43) Diebold, U. The Surface Science of Titanium Dioxide. *Surf. Sci. Rep.* **2003**, *48*, 53−229.
(44) Liu, M.; Piao, L.; Zhao, L.; Ju, S.; Yan, Z.; He, T.; Zhou, C.; Wang, W. Anatase TiO_2 Single Crystals with Exposed {001} and {110} Facets: Facile Synthesis and Enhanced Photocatalysis. *Chem. Commun.* **2010**, *46*, 1664−1666.
(45) Yang, W.; Li, J.; Wang, Y.; Zhu, F.; Shi, W.; Wan, F.; Xu, D. A Facile Synthesis of Anatase TiO_2 Nanosheets-Based Hierarchical Spheres with over 90% {001} Facets for Dye-Sensitized Solar Cells. *Chem. Commun.* **2011**, *47*, 1809−1811.
(46) Anisimov, V. I.; Zaanen, J.; Andersen, O. K. Band Theory and Mott Insulators: Hubbard U instead of Stoner I. *Phys. Rev. B* **1991**, *44*, 943−954.
(47) Dudarev, S. L.; Botton, G. A.; Savrasov, S. Y.; Humphreys, C. J.; Sutton, A. P. Electron-Energy-Loss Spectra and the Structural Stability of Nickel Oxide: An LSDA+U Study. *Phys. Rev. B* **1998**, *57*, 1505−1509.
(48) Morgan, B. J.; Watson, G. W. A DFT+ U Description of Oxygen Vacancies at the TiO_2 Rutile (110) Surface. *Surf. Sci.* **2007**, *601*, 5034−5041.
(49) Ganduglia-Pirovano, M. V.; Hofmann, A.; Sauer, J. Oxygen Vacancies in Transition Metal and Rare Earth Oxides: Current State of Understanding and Remaining Challenges. *Surf. Sci. Rep.* **2007**, *62*, 219−270.
(50) Nolan, M.; Grigoleit, S.; Sayle, D. C.; Parker, S. C.; Watson, G. W. Density Functional Theory Studies of the Structure and Electronic Structure of Pure and Defective Low Index Surfaces of Ceria. *Surf. Sci.* **2005**, *576*, 217−229.

(51) Ferrari, A. M.; Pisani, C.; Cinquini, F.; Giordano, L.; Pacchioni, G. Cationic and Anionic Vacancies on the NiO(100) Surface: DFT+U and Hybrid Functional Density Functional Theory Calculations. *J. Chem. Phys.* **2007**, *127*, 174711.
(52) Long, R.; English, N. J.; Mooney, D. A. Electronic Structures of N- and C-Doped NiO from First-Principles Calculations. *Phys. Lett. A* **2010**, *374*, 1184−1187.
(53) Yu, N.; Zhang, W.-B.; Wang, N.; Wang, W.-F.; Tang, B.-Y. Water Adsorption on a NiO(100) Surface: A GGA+U Study. *J. Phys. Chem. C* **2008**, *112*, 452−457.
(54) Tada, H.; Matsui, H.; Shiota, F.; Nomura, M.; Ito, S.; Yoshihara, M.; Esumi, K. Heterosupramolecular Photocatalysis: Oxidation of Organic Compounds in Nanospaces between Surfactant Bilayers Formed on TiO_2. *Chem. Commun.* **2002**, 1678−1679.
(55) Nolan, M.; Iwaszuk, A.; Tada, H. Molecular Metal Oxide Cluster-Surface Modified Titanium(IV) Dioxide Photocatalysts. *Aust. J. Chem.* **2012**, *65*, 624−632.
(56) Niishiro, R.; Kato, H.; Kudo, A. Nickel and Either Tantalum or Niobium-Codoped TiO_2 and $SrTiO_3$ Photocatalysts with Visible-Light Response for H_2 or O_2 Evolution from Aqueous Solutions. *Phys. Chem. Chem. Phys.* **2005**, *7*, 2241−2245.
(57) Liu, G.; Wang, L.; Yang, H. G.; Cheng, H. -M.; Lu, G. Q. Titania-Based Photocatalysts—Crystal Growth, Doping and Heterostructuring. *J. Mater. Chem.* **2010**, *20*, 831−843.
(58) Serpone, N.; Lawless, D.; Khairutdinov, R. Size Effects on the Photophysical Properties of Colloidal Anatase TiO_2 Particles: Size Quantization versus Direct Transitions in This Indirect Semiconductor. *J. Phys. Chem.* **1995**, *99*, 16646−16654.
(59) Anpo, M.; Takeuchi, M. The Design and Development of Highly Reactive Titanium Oxide Photocatalysts Operating under Visible Light Irradiation. *J. Catal.* **2003**, *216*, 505−516.
(60) Kitano, M.; Funatsu, K.; Matsuoka, M.; Ueshima, M.; Anpo, M. Preparation of Nitrogen-Substituted TiO_2 Thin Film Photocatalysts by the Radio Frequency Magnetron Sputtering Deposition Method and Their Photocatalytic Reactivity under Visible Light Irradiation. *J. Phys. Chem. B* **2006**, *110*, 25266−25272.
(61) Nolan, M.; Tofail, S. A. M. Density Functional Theory Simulation of Titanium Migration and Reaction with Oxygen in the Early Stages of Oxidation of Equiatomic NiTi alloy. *Biomaterials* **2010**, *31*, 3439−3448.
(62) Henkelman, G.; Arnaldsson, A.; Jónsson, H. A Fast and Robust Algorithm for Bader Decomposition of Charge Density. *Comput. Mater. Sci.* **2006**, *36*, 354−360.
(63) Wang, C. M.; Heller, A.; Gerischer, H. Palladium Catalysis of O_2 Reduction by Electrons Accumulated on TiO_2 Particles during Photoassisted Oxidation of Organic Compounds. *J. Am. Chem. Soc.* **1992**, *114*, 5230−5234.
(64) Hoffmann, M. R.; Martin, S. T.; Choi, W.; Bahnemann, D. W. Environmental Application of Semiconductor Photocatalysis. *Chem. Rev.* **1995**, *95*, 69−96.